

## Article

# Experimental and Theoretical Study on the Internal Convective and Radiative Heat Transfer Coefficients for a Vertical Wall in a Residential Building

Piotr Michalak 

Department of Power Systems and Environmental Protection Facilities, Faculty of Mechanical Engineering and Robotics, AGH University of Science and Technology, Mickiewicza 30, 30-059 Kraków, Poland; pmichal@agh.edu.pl; Tel.: +48-126-173-579

**Abstract:** Experimental studies on internal convective (CHTC) and radiative (RHTC) heat transfer coefficients are very rarely conducted in real conditions during the normal use of buildings. This study presents the results of measurements of CHTC and RHTC for a vertical wall, taken in a selected room of a single-family building during its everyday use. Measurements were performed using HFP01 heat flux plates, Pt1000 sensors for internal air and wall surface temperatures and a globe thermometer for mean radiant temperature measured in 10 min intervals. Measured average CHTC and RHTC amounted to 1.15 W/m<sup>2</sup>K and 5.45 W/m<sup>2</sup>K, compared to the 2.50 W/m<sup>2</sup>K and 5.42 W/m<sup>2</sup>K recommended by the EN ISO 6946, respectively. To compare with calculated CHTC, 14 correlations based on the temperature difference were applied. Obtained values were from 1.31 W/m<sup>2</sup>K (given by Min et al.) to 3.33 W/m<sup>2</sup>K (Wilkes and Peterson), and in all cases were greater than the 1.15 W/m<sup>2</sup>K from measurements. The average value from all models amounted to 2.02 W/m<sup>2</sup>K, and was greater than measurements by 75.6%. The quality of models was also estimated using average absolute error (AAE), average biased error (ABE), mean absolute error (MAE) and mean bias error (MBE). Based on these techniques, the model of Fohanno and Polidori was identified as the best with AAE = 68%, ABE = 52%, MAE = 0.41 W/m<sup>2</sup>K and MBE = 0.12 W/m<sup>2</sup>K.

**Keywords:** convection; radiation; heat transfer coefficient; correlation



**Citation:** Michalak, P. Experimental and Theoretical Study on the Internal Convective and Radiative Heat Transfer Coefficients for a Vertical Wall in a Residential Building. *Energies* **2021**, *14*, 5953. <https://doi.org/10.3390/en14185953>

Academic Editor: Paulo Santos

Received: 31 July 2021

Accepted: 15 September 2021

Published: 19 September 2021

**Publisher's Note:** MDPI stays neutral with regard to jurisdictional claims in published maps and institutional affiliations.



**Copyright:** © 2021 by the author. Licensee MDPI, Basel, Switzerland. This article is an open access article distributed under the terms and conditions of the Creative Commons Attribution (CC BY) license (<https://creativecommons.org/licenses/by/4.0/>).

## 1. Introduction

Heat transfer by convection and radiation plays an important role in numerous applications from nanoscale [1–3] to large industrial installations [4]. Among these, buildings are of special interest because of their important contribution to global energy consumption [5]. Therefore, for economic and environmental reasons, it is common for the energy performance of buildings to be legally regulated in many countries [6].

Heat transfer by convection and radiation plays important role in the internal environment of a building, influencing thermal comfort, the operation of heating, ventilation and air conditioning (HVAC) systems, and energy consumption [7–10]. Heat transfer by convection and radiation can be derived both theoretically and experimentally, however the latter method prevails when considering non-typical and more complex cases, or for proving theoretical investigations.

Energy performance assessments for buildings are usually based on the energy usage for the heating and cooling of the space [11], calculated using various computer tools. These tools employ different models to compute radiative and convective heat transfer coefficients. The nature of the physical phenomenon for a given heat transport mechanism determines the parameters necessary to compute the appropriate coefficients. Heat transfer by radiation is simple to describe, as it depends on the temperature, emissivity and position of the considered body and its surroundings. Moreover, numerous studies have proven that the difference between the air and mean radiant temperatures inside the building zone

is relatively small, typically below 2 °C [12], and in practice, constant values of radiative heat transfer coefficients (RHTCs) are commonly used [13,14] to simplify calculations.

In terms of heat transfer by convection, the aforementioned temperatures, flow conditions, and physical properties of the fluid (air) are needed. Hence, mathematical description is more complex than in the previous case, and analytical solutions are available mainly for relatively simple cases. For these reasons, over the past few decades, experimental correlation models of the convective heat transfer coefficients (CHTCs) have been developed. They significantly reduce computation effort by combining an unknown coefficient with the main driving physical factors in given conditions within the studied case. Usually, these models are subdivided into correlations of dimensionless numbers or temperature differences [15,16]. The first type links Nusselt with Grashof and Prandtl numbers in the form of the power equation  $Nu = C (Gr Pr)^n$  with constant  $C$  and  $n$ . In the second case, an equation of the type  $h_c = C (\Delta T)^n$  is used. The latter form is simpler to use because it is founded on an easily measurable quantity, which is temperature and, in certain cases, geometrical parameters (length, area or height of a surface) and air velocity.

Initially, a lack of detailed data forced the use of results from various physical experiments in buildings' thermal calculations. The similarity of buildings' partitions to typical geometric figures resulted in the use of both theoretical and experimental results, obtained mainly for horizontal, vertical, and inclined planes. Many such studies have been developed in recent decades, and different flow regimes have been studied under natural and forced convection.

Fishenden and Saunders [17–19] investigated convective heat transfer for metal (aluminium, copper, platinum, or steel) vertical plates in air, water and mercury. To study the impact of air pressure on that phenomenon, the measurements were conducted in a cylindrical steel test chamber. The temperature difference was up to 55 °C. Finally, the authors gave experimental correlations with dimensionless numbers, with  $n = 1/4$  and  $n = 1/3$  for laminar and turbulent flow, respectively.

McAdams [20] summarised the results of several previous works of various researchers on natural convection and presented correlations for vertical and horizontal plates and cylinders in the form of dimensionless equations with  $n = 1/4$ . In quoted experiments, metal plates were used (aluminium, copper or platinum). He also presented an alignment chart to derive a heat transfer coefficient for the turbulent flow of various gases on vertical surfaces. In the case of so-called ordinary temperatures and atmospheric pressure, simplified dimensional equations with  $n = 1/3$  and  $n = 1/4$  for turbulent and laminar flow, respectively, were given. The same exponent was used by Lewandowski [21,22] for copper plate in glycerine or for water [23].

Based on previous theoretical and experimental works, Churchill and Usagi [24] developed empirical dimensionless correlations with  $n = 9/4$  and  $n = 8/3$  under laminar free and forced convection, respectively, for an isothermal vertical plate. No information on the temperature difference range was given.

As the interest in building modelling has grown, experimental research on heat transfer phenomena in this group of objects has gained increased importance. Related studies commonly test chambers with dimensions similar to typical rooms in buildings.

Correlations for interior surfaces of buildings for vertical glazing (with no radiator under the window), vertical walls (non-heated or near the heat source) and horizontal surfaces (heated floor or cooled ceiling) were presented by Khalifa and Marshall in [25]. Using a two-zone test cell they performed nine experiments covering the most popular heating configurations in buildings under controlled steady-state conditions, as follows: forced convection on the interior surface using a fan, a cell heated by a 1 kW fan heater, a uniformly heated floor, a uniformly heated vertical wall and a uniformly heated edge using a metalized plastic foil, a cell heated by a 1.5 kW oil-filled radiator located opposite the test wall and adjacent to the test wall, and finally with a single glazed window in a test wall with a radiator located beneath and opposite the window.

The larger hot zone represented a large enclosure (such as a living room). It had one vertical wall common with a smaller cold zone built to control the outdoor temperature of the hot zone. A total of 142 tests were conducted. Vertical walls and the roof were covered with aluminium foil to minimise the impact of internal longwave radiative heat exchange on temperature and heat flux measurements, and to neglect it in heat transfer calculations. To reach the steady-state conditions between two consecutive tests with different configurations, a 24 h pre-run period was applied, and then 12 h data logging between 22:00 and 10:00 was undertaken. The CHTCs obtained for each of the different studied elements were presented as dimensional correlations against the internal air to wall surface temperature difference. For the heated vertical wall  $n = 1/4$  was obtained.

Alamdari and Hammond [26] used the model of Churchill and Usagi to derive empirical correlations for buoyancy-driven convective heat transfer for the internal surfaces of naturally ventilated buildings, covering laminar, transitional, and turbulent airflows. They noticed that the experimental results related to buoyancy-driven convection given in the literature were often given for fluids, surface dimensions, and temperature differences not found in buildings. Based on Churchill and Usagi considerations and experiments presented by other researchers, they developed several correlations of different complexity and applicable for vertical and horizontal partitions.

Natural convection from heated surfaces in a room was examined by Awbi and Hatton [27]. Experiments were conducted in a test chamber and a small box. The first experiment was of a similar concept as presented in [25]. The internal layer of vertical walls, ceiling, and floor was of varnished plywood. Five heating plates (0.5 m per 2.3 m) covered with a 2 mm thick aluminium plate (to minimise radiative heat flux) were used to provide surface heating to each tested wall. To minimise the effect of internal longwave radiation, temperature sensors were shielded by small steel tubes. The small test box was a cube with sides of approximately 1 m made of the same materials. Each test was conducted for several hours to reach steady-state conditions. Obtained equations for CHTCs were in the form of power functions of temperature difference. Correlation coefficients were above 0.90, indicating strong dependences.

Delaforce et al. [28] investigated convective heat transfer at internal surfaces using a rectangular test cell with sides of approximately 2 m each. The cell was located on an exposed grassland site and experiments were conducted during winter conditions. External walls were made from bricks and an external layer of expanded polystyrene. Their internal surface had no additional covering layer, so indoor radiative heat transfer was monitored using a radiometer. Temperatures were measured at 5-min intervals. Heating was provided by a 1 kW fan heater. Continuous heating, intermittent heating, and unheated operation were examined separately for the west wall, floor, and ceiling. Before each experiment, authors used a two-day warm-up period with continuous heating. Finally, they did not provide any empirical correlations, but only averaged the numerical values of the calculated CHTCs and compared them with values recommended by the Chartered Institute of Building Service Engineers (CIBSE) Guide. The greatest discrepancies were noticed for a floor and vertical wall, where the measured CHTC was 0.5 and 1.6 W/m<sup>2</sup>K compared to 1.5 and 3.0 W/m<sup>2</sup>K from CIBSE, respectively.

Test chambers can be also used to analyse the performance of selected buildings components under various conditions. Sukamto et al. [29] used this method to investigate the thermal performance of the ventilated wall. Because of forced airflow, the obtained CHTC was about 20 W/m<sup>2</sup>K.

Furthermore, several authors studied the impact of the heating, ventilation and air conditioning systems (HVAC) on internal heat transfer in buildings. A more detailed review of embedded radiant heating/cooling systems is given in [30]. Cholewa et al. [31,32] investigated heated/cooled radiant floor and radiant ceiling using a test chamber. A similar method was used by Acikgoz and Kincay [33] for radiant cooling walls. Hydronic radiant heated walls in a climatic test chamber with a window were investigated in [34]. Guo et al., investigated convective heat transfer for night cooling with diffuse ceiling [35]

and mixing [36] ventilation in a guarded hot box used as a test chamber. To evaluate the dependence of CHTC on ventilation conditions, they used several correlations linking them with ventilation air changes per hour (ACH). Various cases of CHTCs for different building partitions in the form of empirical correlations are given in reviews [10,16,37–40]. For example, in the review by Khalifa, with CHTC correlations derived in 1, 2 and 3-dimensional enclosures [39,40], the author presented 13 studies performed for the latter case. The author concluded that large differences may arise between the presented models.

Recently, and in addition to the aforementioned methods, various computer-based techniques have been developed, and simulation tools used, in convective heat transfer analyses [41–45]. Despite their abilities to deal with complex problems that are not possible to solve analytically, they are used for proving experimental results rather than to formulate mathematical relationships to obtain convection heat transfer coefficients in building applications. For these reasons, in energy auditing, energy certification, or in other similar applications requiring relatively low computational effort and a limited number of input parameters, constant CHTC and RHTC values are commonly used [46,47]. These are given in various standards, such as EN 1264 [48], ISO 11855 [49], EN ISO 6946 [50] and guidebooks [51] providing relevant formulas to obtain CHTC or their constant values in different cases.

The presented methods and techniques more or less accurately reflect the nature of heat transfer phenomena in buildings. They allow the separation of noise, stabilisation, and control of thermal conditions, and so on [52]. On the other hand, the applicability of the theoretical models should be verified in real conditions. For this reason, the best research object seems to be a real building.

Cost, practical problems, and limitations for building users resulting from the presence of measuring equipment in the building during its everyday use are the probable reasons for so few tests being carried out in these conditions. Hence, there are few CHTCs from experiments in realistic situations [53]. Most measurements have been made in special test chambers where internal surfaces were metal coated. Therefore, it seems reasonable to address indoor convective and radiative heat transfer in buildings during their everyday use.

Wallentén [53] experimentally analysed internal convective heat transfer at an external wall with a window in a room with and without furniture, located in a single-family house built in a sandwich construction of light-weight concrete and polystyrene. The room had the dimensions of  $3 \times 3.6 \times 2.4$  m. Internal surfaces of walls and floor were painted with a mat white and light brown colour, respectively. Two electric radiators with 500 W and 1000 W heating power were used. T-type thermocouples were used to measure indoor air and partition temperatures. Longwave radiation was calculated from diffuse grey surface temperatures. A total of 14 different experiments (radiator placement, presence of furniture, wall and window analysis, ventilation schedule), each lasting approximately one week, were performed across four years. A sampling time of 1 min was assumed and then measurements were averaged in 4, 10, 30 and 60 min intervals. The author did not provide any conclusions on the impact of the averaging time on final results. Several graphs with CHTC depending on the surface (vertical wall or window) and indoor air temperature were presented, but no correlations were given. As far as the wall is concerned, the data from measurements were quite scattered and showed little correlation. The spatial distribution of internal air temperature was also presented. An impact from the radiator or ventilation was visible, but the maximum difference between the floor and ceiling did not exceed  $3^\circ\text{C}$ . Only near the window, at a distance of several cm, it reached  $5^\circ\text{C}$ .

The review presented here shows several important outcomes. Thermal conditions in climatic chambers during the aforementioned tests were controlled according to the requirements necessary to perform the assumed tests. Noises could be easily limited using selected construction materials or HVAC system components. On the other hand, heat transfer in buildings during everyday use is influenced by different environmental factors, such as occupation, solar radiation, air ventilation, and so on. The very low number

of studies dedicated to this issue makes it worthy to compare the models developed theoretically or on a basis of experiments in test chambers, with those derived from real conditions in a building during its normal operation. The identification of the most significant limitations during such an experiment is also a possibility, and could indicate possible improvements to similar studies in the future.

The environmental conditions during measurements and experimental setup are given in the next section. Calculation procedures to obtain CHTC and RHTC and uncertainty analysis are then presented. For comparative purposes, 14 theoretical and empirical correlations to obtain CHTC for a vertical wall under free convection are used. The results are then presented and compared with relevant studies. Finally, concluding remarks are given.

## 2. Materials and Methods

### 2.1. Introduction

The research was conducted from 30 January to 10 February 2021 in a residential building located in southern Poland, equipped with a hydronic heating system.

During the studied period the outdoor air temperature (Figure 1) varied from  $-15.1\text{ }^{\circ}\text{C}$  (at 3:50 on 1 February) to  $10.1\text{ }^{\circ}\text{C}$  (at 9:30 on 4 February). Global solar irradiance (Figure 2) incident on the external surface of the considered wall was from 0 to  $113.3\text{ W/m}^2$  (at 13:20 on 31 January).

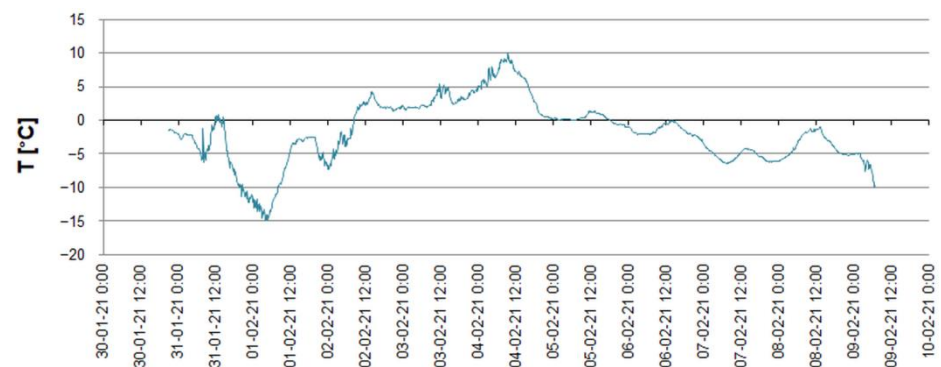


Figure 1. External air temperature during measurements.

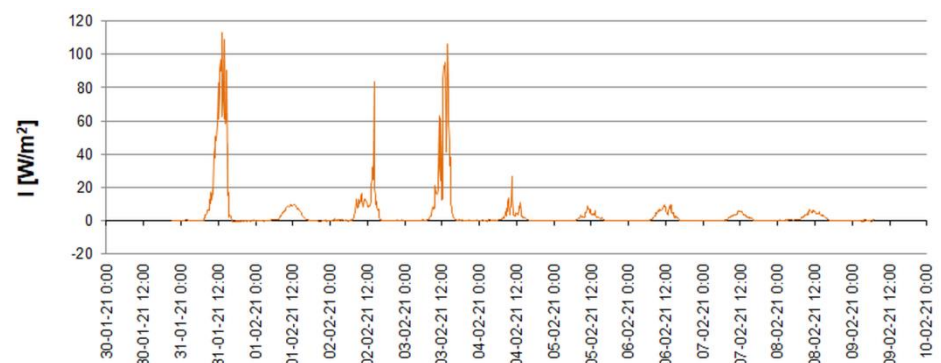
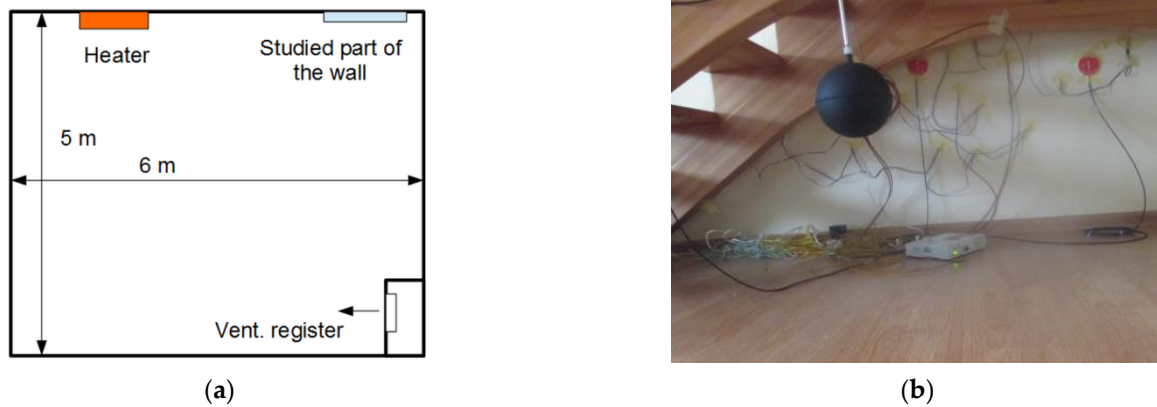


Figure 2. Global solar irradiance on the west-facing wall during measurements.

### 2.2. Experimental Setup

The west-oriented wall (strictly—its north part) in a living room was chosen for the measurements (Figure 3). Also located in this corner of the room are wooden stairs. The room is on a rectangular plane of  $6\text{ m} \times 4\text{ m}$  and has a height of 2.50 m.



**Figure 3.** (a) View of the room selected for experiment; (b) View of the measurement equipment during assembly.

The measured data was recorded in 10 min intervals with a MS6D Comet data logger. Periods from 4 to 60 min have typically been used in other studies [25,28,53].

In the experiment, two HFP01 heat flux sensors and three Pt1000 temperature sensors were mounted on the internal surface of the wall, while two Pt1000 internal air temperature sensors, one sensor of indoor radiant ( $\varnothing$  150 mm TP875.1 globe thermometer with the Pt100 sensor) and one Pt1000 of outdoor air temperature (mounted in a radiation shield) and a CMP11pyranometer for global solar irradiance incident were placed on the external wall. Their main parameters are given in Table 1.

**Table 1.** The main metrological parameters of the measuring sensors used.

Sensor	Measured Variable	Measurement Range	Accuracy
Pt1000 platinum resistance sensor	Air temperature	$-50\text{ }^{\circ}\text{C} \div +150\text{ }^{\circ}\text{C}$	Class A <sup>1</sup>
Pt1000 platinum resistance sensor	Wall surface temperature	$-50\text{ }^{\circ}\text{C} \div +150\text{ }^{\circ}\text{C}$	Class A <sup>1</sup>
TP875.1 with the Pt100 sensor	Radiant temperature	$-30\text{ }^{\circ}\text{C} \div +120\text{ }^{\circ}\text{C}$	$\pm 0.2\text{ }^{\circ}\text{C}$
CMP11 Kipp&Zonen	Solar irradiance	$0 \div 4000\text{ W/m}^2$	Spectrally Flat Class A <sup>2</sup>
HFP01 Hukseflux	Heat fluxdensity	$-2000 \div 2000\text{ W/m}^2$	$\pm 3\%$

<sup>1</sup> According to EN 60751. <sup>2</sup> According to ISO 9060 and IEC 61724.

### 2.3. Calculation Procedure

The conduction heat flux flowing through the wall ( $q_w$ ) and measured by the heat flux sensors (Figure 1) is the sum of radiative ( $q_r$ ) and convective ( $q_c$ ) fluxes entering an interior space of the room:

$$q_w = q_r + q_c. \quad (1)$$

The radiative heat flux is given by the relationship:

$$q_r = h_r(T_s - T_r), \quad (2)$$

Within the building enclosure, the considered wall at temperature  $T_s$  is exposed to remaining walls and heat transfer by radiation occurs between them. The mean radiant temperature of the given wall surroundings is measured by the globe thermometer [28–30]. Then, based on the Stefan–Boltzmann law and at the given emissivity of the wall,  $\epsilon$ , the following equation can be written [31]:

$$q_r = \epsilon\sigma(T_s^4 - T_r^4). \quad (3)$$

Comparing Equations (2) and (3) we obtain:

$$h_r = \epsilon\sigma \frac{T_s^4 - T_r^4}{T_s - T_r} = \epsilon\sigma(T_s + T_r)(T_s^2 + T_r^2). \quad (4)$$

Equation (4) shows that  $h_r$  can be obtained without direct measurement of radiative heat flux.

Convective heat flux is given by:

$$q_c = h_c(T_s - T_i). \quad (5)$$

With  $q_r$  known,  $q_c$  can be obtained from Equation (1), and then, from Equation (5) an unknown convective heat transfer coefficient can be computed.

#### 2.4. Uncertainty Analysis

Experimental investigations inevitably have associated measurement errors. Both RHTC and CHTC are computed in the present study indirectly from formulas given by Equations (4) and (5), respectively.

In cases where the indirect measurement of a physical quantity,  $y$ , is a function of independent measurements  $x_1, x_2, \dots, x_n$ :

$$y = f(x_1, x_2, \dots, x_n) \quad (6)$$

the standard combined uncertainty  $u_c$  of  $y$  can be calculated applying the propagation model of uncertainty from the formula [54–59]:

$$u_c(y) = \sqrt{\left(\frac{\partial y}{\partial x_1} u(x_1)\right)^2 + \left(\frac{\partial y}{\partial x_2} u(x_2)\right)^2 + \dots + \left(\frac{\partial y}{\partial x_n} u(x_n)\right)^2}. \quad (7)$$

In the next step, the expanded uncertainty of the measured quantity is calculated from the equation:

$$U = k u_c(y) \quad (8)$$

where  $k$ —coverage factor;  $k = 2$  for 95% confidence level of the uncertainty.

Following the calculation procedure presented in the previous section, the uncertainty of RHTC is derived. From Equation (4) we obtain:

$$h_r = \varepsilon \sigma (T_s^3 + T_s T_r^2 + T_r T_s^2 + T_r^3). \quad (9)$$

Inserting Equation (9) into Equation (7) we get an expression to obtain the standard combined uncertainty of the measured RHTC. Three independent variables can be distinguished, namely:  $\varepsilon$ ,  $T_r$  and  $T_s$ . Hence, Equation (7) can be written as:

$$u_c(h_r) = \sqrt{\left(\frac{\partial(h_r)}{\partial \varepsilon} u(\varepsilon)\right)^2 + \left(\frac{\partial(h_r)}{\partial T_r} u(T_r)\right)^2 + \left(\frac{\partial(h_r)}{\partial T_s} u(T_s)\right)^2}. \quad (10)$$

Then, partial derivatives in Equation (10) are computed, as follows:

$$\frac{\partial h_r}{\partial \varepsilon} = \sigma (T_s^3 + T_s T_r^2 + T_r T_s^2 + T_r^3), \quad (11)$$

$$\frac{\partial h_r}{\partial T_r} = \varepsilon \sigma (2T_s T_r + T_s^2 + 3T_r^2), \quad (12)$$

$$\frac{\partial h_r}{\partial T_s} = \varepsilon \sigma (3T_s^2 + T_r^2 + 2T_s T_r). \quad (13)$$

The uncertainty associated with the measurement of emissivity, mean radiant temperature and surface temperature can be derived based on sensors and measurement equipment data presented in Section 2.2.

The estimation of emissivity uncertainty is a very difficult task. Several authors have presented methods to address this issue, involving different approaches. Ficker [60] used

two precise black body etalons of different emissivities heated to the same temperature to develop a comparative method to estimate virtual emissivity of infrared (IR) thermometers. Chen and Chen [61] determined the emissivity and temperature of construction materials by using an IR thermometer and two contact thermometers. For this purpose, they developed empirical regression equations. Höser et al. [62] found unknown emissivities of rock samples by comparing the temperature of the tested samples with a reference sample at a known temperature. They concluded that the relative uncertainty in rock emissivity is proportional to the relative uncertainty in the rock temperature ( $T$ ) in the absolute sale. It can be written as:

$$u(\varepsilon) = \left| -4 \frac{u(T)}{T} \varepsilon \right|, \quad (14)$$

This method seems to be the most appropriate in the considered case and was applied here.

The remaining uncertainties of two temperatures,  $T_r$  and  $T_s$ , are both comprised of two elements. The first results from the accuracy of a temperature sensor. The latter is the effect of the data logging device accuracy [55,63]. Hence, we obtain:

$$u(T_r) = \sqrt{(u_{\text{sens},r})^2 + (u_{\text{dev},r})^2}, \quad (15)$$

and:

$$u(T_s) = \sqrt{(u_{\text{sens},s})^2 + (u_{\text{dev},s})^2}, \quad (16)$$

where “sens” and “dev” subscripts refer to sensor and measuring device, respectively. Subscripts after a comma,  $r$  and  $s$ , refer to radiant temperature and surface temperature, respectively.

Similar considerations should be made to obtain CHTC uncertainty. Firstly, Equation (5) is rearranged to the form:

$$h_c = \frac{q_c}{T_s - T_i}. \quad (17)$$

In the above formula, three independent variables can be distinguished that influence measured CHTC, i.e.,  $q_c$ ,  $T_i$  and  $T_s$ . Then, the uncertainty of CHTC is given by:

$$u_c(h_c) = \sqrt{\left( \frac{\partial(h_c)}{\partial q_c} u(q_c) \right)^2 + \left( \frac{\partial(h_c)}{\partial T_i} u(T_i) \right)^2 + \left( \frac{\partial(h_c)}{\partial T_s} u(T_s) \right)^2}. \quad (18)$$

Subsequent partial derivatives are as follows:

$$\frac{\partial h_c}{\partial q_c} = \frac{1}{T_s - T_i}, \quad (19)$$

$$\frac{\partial h_c}{\partial T_s} = \frac{-q_c}{(T_s - T_i)^2}, \quad (20)$$

$$\frac{\partial h_c}{\partial T_i} = \frac{q_c}{(T_s - T_i)^2}. \quad (21)$$

The uncertainty associated with the measurement of indoor air temperature  $u(T_i)$  and surface temperature ( $T_s$ ) can be derived similarly, as in the previous case on the basis of Equations (15) and (16). However, a measurement of heat flux density requires some additional explanation. In this case, according to the manufacturer’s manual [64], measurement uncertainty consists of several components. These are calibration uncertainty, the difference between measurement and reference calibration conditions, the duration of sensor employment, and application errors resulting from working conditions. They can be included in the relationship:

$$u(q_c) = \sqrt{\sum_{i=1}^n u_i^2}, \quad (22)$$

where  $n$  is the number of uncertainty components and  $u_i$  is the  $i$ -th component.

### 2.5. Selected Correlations for CHTC Calculations

During the test, there was no measured air velocity near the wall. A gravity ventilation system is present in the building, but the ventilation register in the room, however, is located far from the studied wall and was closed, and it was assumed that it has no impact on the flow regime near the wall. Hence, for further consideration, 13 correlations were chosen to obtain convective heat transfer coefficients for vertical walls under natural convection [10,16,37,65,66]. In all following relationships, it is assumed that:

$$\Delta T = T_s - T_i. \quad (23)$$

The model of Wilkes and Peterson (quoted from [16]) is given by:

$$h_c = 3.05(\Delta T)^{0.12}. \quad (24)$$

In [19] it was stated that that model was developed on the basis of a test for temperature difference between 4.5 to 15.5 °C with two heated plates 2.4 × 0.8 m with 0.1 m air space. The resulting correlation was derived on the three data points only.

Khalifa in his review [39] quoted the relationship developed originally by Hottinger:

$$h_c = 2.50(\Delta T)^{1/4}. \quad (25)$$

Min et al. [40] determined natural convection coefficients by using three different sized rectangular test chambers. Hence, they are not applicable in the considered case. For the vertical wall, they obtained correlations in the case of the heated ceiling and heated floor. They also referred to other correlations from various other studies. The first of these, presented here, was developed using a 0.60 m square plate, the temperature difference up to 555 °C and the height  $H$ . For laminar flow:

$$h_c = 1.368 \left( \frac{\Delta T}{H} \right)^{1/4}. \quad (26)$$

The second correlation was developed during tests with a 1.2 m square plate. Apart from the temperature difference up to 100 °C, no additional information on the application range was given. The model was given by two equations, as follows:

$$h_c = 1.776(\Delta T)^{1/4} \quad (27)$$

and for the turbulent flow:

$$h_c = 1.973(\Delta T)^{1/4}. \quad (28)$$

The third is the correlation from King. Unfortunately, no data related to the test details or applicability ranges were provided. It is given by:

$$h_c = 1.517(\Delta T)^{1/3}. \quad (29)$$

Alamdari and Hammond [26] derived correlations for convective heat transfer from the internal surfaces in naturally ventilated buildings. Using data from other studies, and applying the mathematical model of Churchill and Usagi [24], they proposed the following relationship:

$$h_c = \left\{ \left[ 1.5 \left( \frac{\Delta T}{L} \right)^{1/4} \right]^6 + \left[ 1.23(\Delta T)^{1/3} \right]^6 \right\}^{1/6}. \quad (30)$$

In addition, they provided a simplified formula valid within the limited range of temperatures and applicable to naturally ventilated buildings, given by the expression:

$$h_c = 0.134L^{-1/2} + 1.11(\Delta T)^{1/6}, \quad (31)$$

where L is a hydraulic diameter expressed as:

$$L = 4A/P \quad (32)$$

Fohanno and Polidori [67] analysed laminar and turbulent heat transfer modelling at uniformly heated internal vertical building surfaces. The resulting correlations for CHTC were derived theoretically and compared with other models. Their model is given by the equation:

$$h_c = 1.332 \left( \frac{\Delta T}{H} \right)^{1/4}. \quad (33)$$

Musy et al. [68], quoting the work of Allard, presented the following equation for walls with natural convection:

$$h_c = 1.5(\Delta T)^{1/3}. \quad (34)$$

Churchill and Chu [65] investigated uniformly heated and cooled vertical plates. Their correlation is given by:

$$h_c = \frac{0.0257}{H} \left( 0.825 + 7.01(\Delta T)^{1/6} H^{3/6} \right)^2. \quad (35)$$

Khalifa and Marshall [25] investigated internal convection in a real-sized indoor test cell. Various combinations of relative positions of a heater, radiant panels and wall were studied. Two cases similar to that studied in the present paper were chosen. The first one is the case with a room heated by a radiator located adjacent to the test wall:

$$h_c = 2.20(\Delta T)^{0.21}. \quad (36)$$

The second is a room heated by an oil-filled radiator located under a window:

$$h_c = 2.35(\Delta T)^{0.21}. \quad (37)$$

Rogers and Mayhew [69] presented the correlation for vertical plates under laminar or transitional flow conditions:

$$h_c = 1.42 \left( \frac{\Delta T}{H} \right)^{1/4}. \quad (38)$$

## 2.6. Statistical Analysis

Additionally, various statistical measures can be used to perform error analysis of the presented models against measured CHTC [70]. Among them, there is an average absolute error (AAE), average biased error (ABE), mean absolute error (MAE) and mean bias error (MBE) [71,72]. Assuming that  $h_{m,i}$  is a  $i$ -th measured value of CHTC,  $h_{p,i}$  is a  $i$ -th value of CHTC predicted by the model and  $m$  is a total number of conducted measurements, they are given by the following equations:

$$AAE = \frac{1}{m} \sum_{i=1}^m \frac{|h_{p,i} - h_{m,i}|}{h_{m,i}} \times 100\%, \quad (39)$$

$$ABE = \frac{1}{m} \sum_{i=1}^m \frac{(h_{p,i} - h_{m,i})}{h_{m,i}} \times 100\%, \quad (40)$$

$$\text{MAE} = \frac{1}{m} \sum_{i=1}^m |h_{p,i} - h_{m,i}|, \quad (41)$$

$$\text{MBE} = \frac{1}{m} \sum_{i=1}^m (h_{p,i} - h_{m,i}). \quad (42)$$

The average absolute error (AAE) is the average of all the absolute errors calculated for the consecutive measurements in a given dataset, and indicates the average error of a correlation. The average biased error (ABE) shows the degree of overestimation ( $\text{ABE} > 0$ ) or underestimation ( $\text{ABE} < 0$ ) of the considered correlation. The mean absolute error (MAE) shows the average magnitude of deviations of a modelled variable against the reference values. Low MAE indicates the high accuracy of a model. MBE is used to determine the overall bias of the correlation. Positive MBE means the overestimation of the model.

### 3. Results and Discussion

#### 3.1. Radiative Heat Transfer Coefficient

##### 3.1.1. Introduction

The radiative heat transfer coefficient was computed from Equation (4). During the whole period, the radiant temperature was higher than that of the wall surface (Figure 4). This difference varied from 1.54 °C (at 13:10 on 7 February) to 0.28 °C (at 6:50 on 6 February), with an average of 0.91 °C.



Figure 4. Average wall surface temperature ( $T_s$ ) and radiative temperature ( $T_r$ ).

RHTC, calculated under the aforementioned conditions, varied during the measurement period (Figure 5) from 5.373 W/m<sup>2</sup>K (at 16:40 on 3 February) to 5.516 W/m<sup>2</sup>K (at 21:00 on 31 January), with an average of 5.445 W/m<sup>2</sup>K. The EN ISO 6946 standard [50] gives the value  $h_r = 5.7$  W/m<sup>2</sup>K for the blackbody at 20 °C. Consequently, for  $\epsilon = 0.95$  resulting  $h_r = 5.415$  W/m<sup>2</sup>K is very close to that average value.

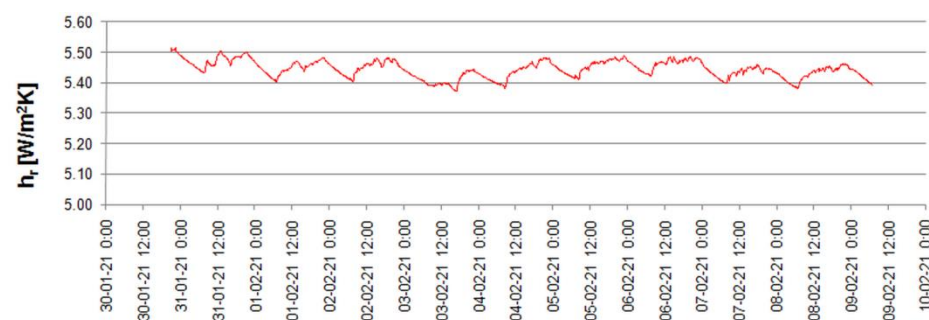


Figure 5. Radiative heat transfer coefficient from measurements.

Assuming that:

$$T_m = 0.5 (T_r + T_s) \quad (43)$$

For cases with small  $T_m$  values, Equation (4) can be linearised [73,74] to the form:

$$h_r = 4\varepsilon\sigma T_m^3. \quad (44)$$

Despite the nonlinear dependence of the RHTC on  $T_m$ , given by Equation (44),  $h_r$  almost linearly changes with  $T_s$  (Figure 6). This occurs primarily because of the relatively narrow range of  $T_s$  variation within the range below 2.5 °C. Similar observations were reported by Evangelisti et al. [65].

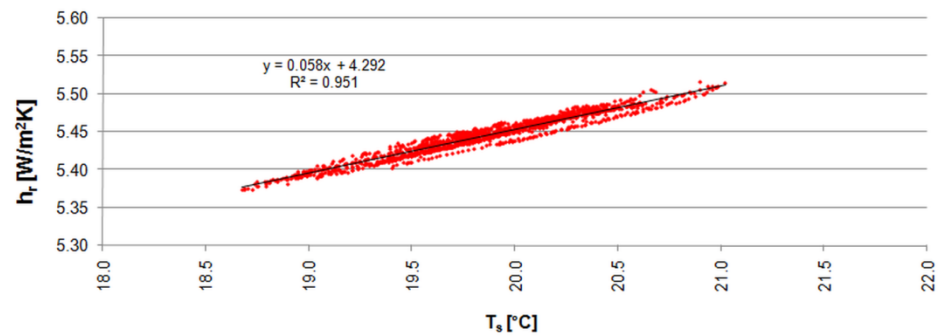


**Figure 6.** Radiative heat transfer coefficient from measurements.

### 3.1.2. Uncertainty Analysis

Before the calculations were made, the emissivity of the internal walls was assumed at  $\varepsilon = 0.95$ . This value was confirmed using a DIT-130 IR-thermometer (declared accuracy  $\pm 1.5\%$  of a measured value + 2 °C) and the reference DFT-700 thermometer with a K-type thermocouple probe (accuracy  $\pm 0.2\%$  of a full scale). Because of its low variation under the conditions considered here, it was reasonable to assume a constant emissivity value of the wall surfaces [75].

Based on the manufacturers' manuals, and assuming a temperature of 25 °C, relevant uncertainties were computed (Table 2). The resultant uncertainty of RHTC measurements is  $u_c(h_r) = 0.18046$  W/m<sup>2</sup>K. Applying coverage factor  $k = 2$  (see Equation (8)) we obtained the expanded uncertainty  $U(h_r) = 0.36$  W/m<sup>2</sup>K. Assuming a temperature of 20 °C the value of  $U(h_r) = 0.34$  W/m<sup>2</sup>K was obtained.

**Table 2.** Uncertainties in RHTC measurement.

Uncertainty	Value	Unit
$u(\varepsilon)$	0.030	—
$u(T_r)$	0.200	K
$u(T_s)$	0.200	K
$\frac{\partial(h_r)}{\partial\varepsilon}$	0.18033	W/m <sup>2</sup> K
$\frac{\partial(h_r)}{\partial T_r}$	0.004788	W/m <sup>2</sup> K <sup>2</sup>
$\frac{\partial(h_r)}{\partial T_s}$	0.004788	W/m <sup>2</sup> K <sup>2</sup>

## 3.2. Convective Heat Transfer Coefficient

### 3.2.1. Introduction

The measured internal air temperature varied from 20.44 °C (at 16:40 on 3 February) to 23.40 °C (at 22:10 on 30 January), with an average of 21.98 °C. It was higher than that of the wall surface (Figure 7). This difference varied from 1.54 °C (at 13:10 on 7 February) to 0.28 °C (at 6:50 on 6 February), with an average of 0.91 °C.

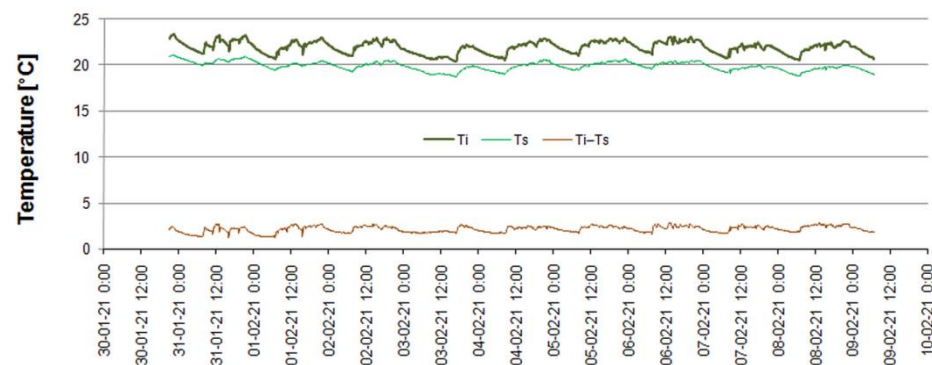


Figure 7. Wall surface temperature ( $T_s$ ), internal air temperature ( $T_i$ ) and their difference.

The calculated CHTC varied throughout the whole period (Figure 8) from  $0.069 \text{ W/m}^2\text{K}$  (at 6:30 on 5 February) to  $3.027 \text{ W/m}^2\text{K}$  (at 14:10 on 2 February), with an average of  $1.153 \text{ W/m}^2\text{K}$ . The EN ISO 6946 standard gives the value  $h_c = 2.5 \text{ W/m}^2\text{K}$  for the internal surface of the vertical wall. The recommended internal surface resistance in such a case is  $R_{si} = 0.13 \text{ m}^2\text{K/W}$ . Taking the measured average  $h_r = 5.445 \text{ W/m}^2\text{K}$  we obtain  $R_{si} = 0.15 \text{ m}^2\text{K/W}$ .

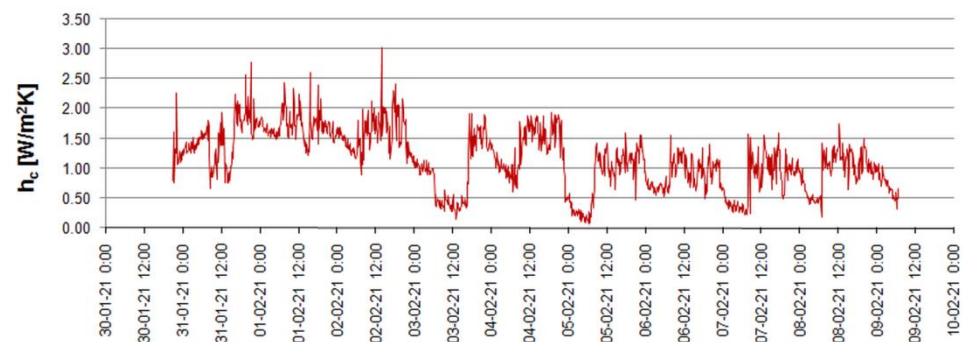


Figure 8. Convective heat transfer coefficient from measurements.

### 3.2.2. Uncertainty Analysis

At first, the uncertainty of the heat flux density measurement should be determined (Equation (22)). In the present study, two HFP sensors were used. Several authors have presented various experimental studies on the thermal performance of buildings using that sensor [76–78], but none of them discussed the problem of heat flux density measurement uncertainty. In some cases, the measurement accuracy of the HFP01 heat flux plate was assumed from 5% [79] to 20% [80]. For this reason, this issue is presented here in detail.

Following recommendations given by the manufacturer [64], the following factors were distinguished:

- calibration uncertainty given by the manufacturer:  $<3\%$  ( $k = 2$ ),
- non-stability uncertainty:  $<1\%$  for every year of operation,
- correction of the resistance error,
- correction of the deflection error,
- error from the temperature dependence:  $<0.1\%$  per  $1^\circ\text{C}$  deviation from the  $20^\circ\text{C}$ .

The calibration, non-stability and temperature errors are relatively easy to estimate because of clear criteria given by the manufacturer. The first is given as expanded uncertainty (see Equation (8)), and for uncertainty budget calculation it was assumed as 1.5%. The latter should be estimated for the worst conditions during measurement, i.e., the greatest temperature measured during the test:  $T_i = 23.40^\circ\text{C}$ .

The resistance error is related to the influence of the sensor thermal resistance added to the resistance of a given partition on the resultant heat flux density. While the manufacturer does not recommend the use of thermal paste because it tends to dry out, it was

applied here because of the relatively short measurement period and moderate temperature. Assuming an average thickness of this paste of 0.1 mm and a thermal conductivity of 1.5 W/m·K it gives the additional thermal resistance of  $6.67 \times 10^{-6} \text{ m}^2\text{K/W}$  in comparison to  $71 \times 10^{-4} \text{ m}^2\text{K/W}$  of the sensor specified by the manufacturer. Hence, the resulting resistance is 0.93%.

Deflection error (called operational error in ISO9869) appears as a result of the difference between the thermal conductivity of the surrounding environment and that of a sensor. The sensor thermal conductivity is 0.76 W/m·K and is in the same order as values typically met in buildings materials: 0.3–0.4 W/m·K for ceramic blocks and 0.7–0.9 W/m·K for cement-lime plaster. Assuming a thermal resistance of the wall of approximately 4 m<sup>2</sup>K/W, we can see that the deflection error is at a negligible level. The average measured heat flux density of 7.42 W/m<sup>2</sup> calculated  $u(q_c) = 0.1526 \text{ W/m}^2$ .

The derivative components, given by Equations (19)–(21), were computed for the most unfavourable conditions during the experiment, i.e., the smallest  $T_s - T_i$ , which amounted to 1.23 °C for  $q_c = 2.54 \text{ W/m}^2$ . Results are given in Table 3. Calculated  $u_c(h_c) = 0.475218 \text{ W/m}^2$ . Taking  $k = 2$  (see Equation (8)) we get a resulting  $U(h_c) = 0.95 \text{ W/m}^2\text{K}$ . On the other hand, for the maximum temperature difference of 2.77 °C and  $q_c = 2.11 \text{ W/m}^2$  the resulting uncertainty is  $U(h_c) = 0.16 \text{ W/m}^2\text{K}$ . Other authors estimated the accuracy of experimentally measured CHTCs from approximately 20% [22,26] to 30% or even 35% at  $\Delta T \approx 1 \text{ °C}$  [53].

**Table 3.** Uncertainties in CHTC measurement.

Uncertainty	Value	Unit
$u(q_c)$	0.05224	W/m <sup>2</sup>
$u(T_i)$	0.200	K
$u(T_s)$	0.200	K
$\frac{\partial(h_c)}{\partial q_c}$	0.81169	W/m <sup>2</sup> K
$\frac{\partial(h_c)}{\partial T_i}$	0.65884	W/m <sup>2</sup> K <sup>2</sup>
$\frac{\partial(h_c)}{\partial T_s}$	0.65884	W/m <sup>2</sup> K <sup>2</sup>

### 3.2.3. Comparison with Other Models

It can be noticed that fluctuations of the CHTC were connected with variations in the difference between internal air and wall surface temperature (Figure 9), but this relationship was rather weak (calculated coefficient of determination  $R^2 = 0.2498$ ). Some authors recommended the use of nonlinear correlations [81,82], but they did not improve the quality of the fit. In case of the logarithmic, exponential, quadratic function and 4-th order polynomial,  $R^2 = 0.2252, 0.2459, 0.2308, \text{ and } 0.2323$ , respectively.

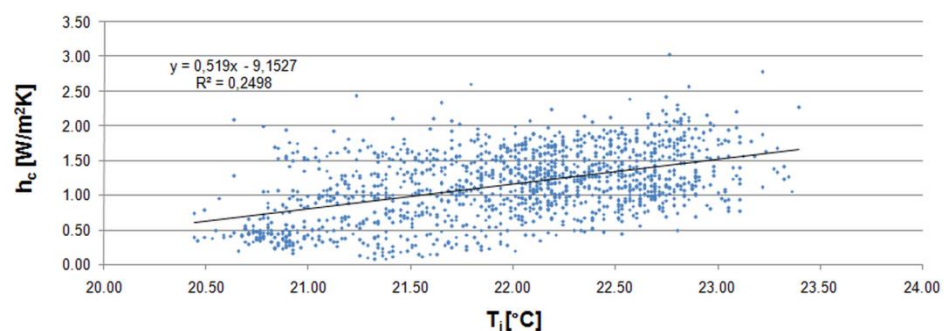


**Figure 9.** Convective heat transfer coefficient versus indoor air temperature.

There are several reasons for this. In the experimental studies performed in test chambers [7,25,27,39,40], thermal conditions during the measurements were stable. As noted in Section 2.5, the ventilation register in the room was closed, however, and located far from the studied wall, and it was assumed that it has no impact on the flow regime

near the wall. The hydronic heater was located approximately 4 m from the measurement equipment. Solar irradiance incident on the external wall was very low (Figure 2), and that falling on internal surfaces could be neglected without any doubt, due to its reduction through windows and curtains. On the other hand, because of the everyday use of the building during the experiment, there could be disturbances in the airflow due to the movement of people in the building, however, indoor air temperature variation was below 3 °C. Hence, to find a solution to this problem, technical factors should be taken into account. Considerations presented in Section 2.4 indicate that an error of CHTC estimation results from uncertainty of heat flux density and air and surface temperature measurement. In the present case, the most important influence was that of the  $T_s - T_i$  temperature difference (Table 3). Both temperatures were measured by accurate sensors (Table 1). However, their difference is in the denominator of the fraction to calculate their uncertainty (Equations (19)–(21)). Hence, not only is the uncertainty of temperature measurement important, but the uncertainty of the temperature difference is as well. In the present study,  $\Delta T$  varied from 1.23 °C to 2.77 °C. These were low values, difficult to measure with high accuracy and which, in certain cases, may lead to unacceptable uncertainties [83]. Numerous studies have pointed out this problem [84–86], and a common practice is to filter out the data when  $\Delta T$  was lower by several Celsius degrees (typically 2–5 °C). This problem should be, however, investigated in more detail in the next experiment.

Several studies have presented the results of experiments on convection at vertical walls at temperature differences below 3 °C. In [26], the heat transfer coefficient for buoyancy-induced airflow near vertical surfaces for  $\Delta T$  of 1 to 10 °C was between 1.5 to 4 W/m<sup>2</sup>K. Khalifa [40] presented the results of numerous experimental and theoretical works on convection at various surfaces. For a vertical wall at  $\Delta T = 2$  °C, CHTC was between 1.2 to 3.0 W/m<sup>2</sup>K. CHTC in a wall with an intermittently heated room [28] was between about 0.2 to 1.5 W/m<sup>2</sup>K during the non-heating period. At continuous heating, the average CHTC was 1.6 W/m<sup>2</sup>K, with a variation between maximum–minimum values of about 1.5 W/m<sup>2</sup>K. CHTC for the temperature difference below 2 K was between 0.2 to 2.5 W/m<sup>2</sup>K. The author did not provide any empirical correlation for  $h_c$ , and only compared averaged values with that recommended by the relevant standards. This significant dispersion of experimental results in a real building was also confirmed in [53]. CHTC was measured in that study at a wall with a radiator at the back wall and no ventilation, and varied from approximately 0.3 to 5.0 W/m<sup>2</sup>K at  $\Delta T < 2$  °C. The dominant results for a wall temperature measured at half of its height ranged between 0.5 and 2.0 W/m<sup>2</sup>K.

CHTC calculated from the 14 correlations presented in Section 2.5 varied from 1.305 W/m<sup>2</sup>K (Equation (26)) to 3.328 W/m<sup>2</sup>K (Equation (24)). In all cases, it was greater than measurements by 1.153 W/m<sup>2</sup>K (Figure 10). The average value from all models was  $h_c = 2.024$  W/m<sup>2</sup>K and was greater than measurements by 75.6%. The results closest to the measured value were obtained for models given by the Equations (26), (31), (33) and (38) and they were greater than measurements by 13.4%, 14.9%, 10.2% and 17.5%, respectively.

Six correlations, given by Equations (26), (30), (31), (33), (35) and (38), included geometrical parameters of the considered wall (hydraulic diameter or height). The relevant columns in Figure 9 were filled with hatching. CHTC in this group of models varied from 1.271 W/m<sup>2</sup>K (Equation (33)) to 1.829 W/m<sup>2</sup>K (Equation (35)), with an average of 1.313 W/m<sup>2</sup>K. The remaining eight models produced results from 1.912 W/m<sup>2</sup>K (Equation (34)) to 3.328 W/m<sup>2</sup>K (Equation (24)), with an average of 2.446 W/m<sup>2</sup>K, i.e., more than twice the measured CHTC. The results presented here indicate that better compliance with measurements was obtained for models that take into account the geometry of the wall.

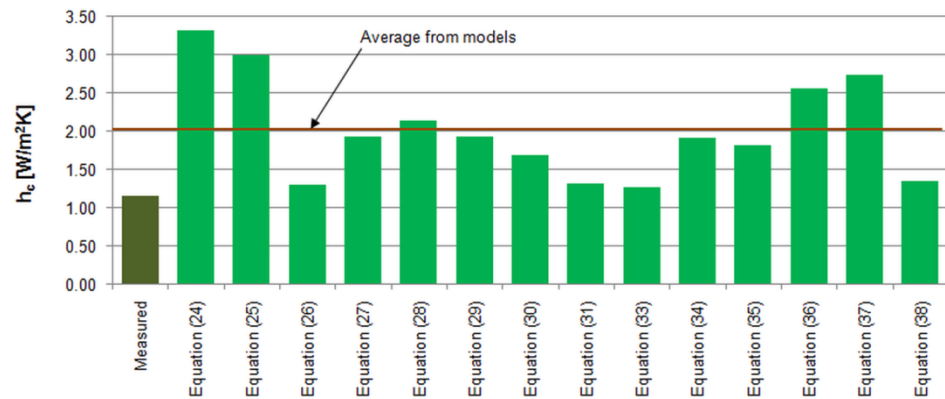


Figure 10. Average ChTC for different models for measurement conditions.

The theoretical calculation of ChTC revealed that various models provide similar results for  $\Delta T$  up to 10 K (Figure 11). These can be gathered into several groups. The first consists of models given by Equations (26), (31), (33) and (38). All except for Equation (31) have an  $(\Delta T/H)^{1/4}$  element. In Equation (31),  $(\Delta T)^{1/6}$  was used along with  $L^{-1/2}$  and resulted in a slightly lower rise in ChTC with  $\Delta T$ . Similarities can also be distinguished between models given by Equations (27) and (28), by (36) and (37), and by (29), (30), (34) and (35).

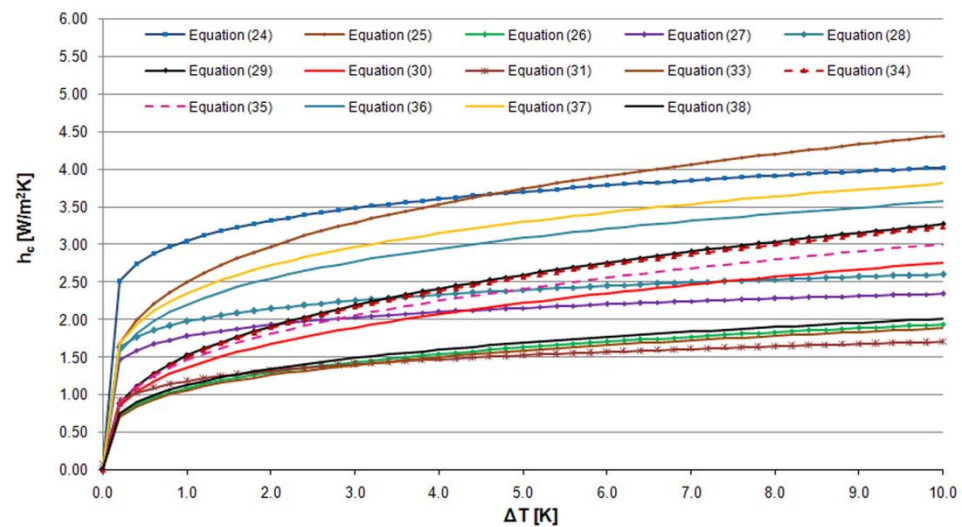


Figure 11. ChTC for different models.

All the models studied here had low coefficients of determination against measurements (Table 4). Their value in the case of the 10 min sampling time did not exceed  $R^2 = 0.0437$  for the linear regression equation. In the next step, hourly averaged values of ChTCs (the typical length of the simulation time step in the building simulation tools) were computed from 10 min variables. The  $R^2$  increase was negligible, in the third decimal place.

**Table 4.** Convective heat transfer coefficients from presented models and coefficients of the determination referred to measured values.

Model (Equation)	$h_c$ [W/m <sup>2</sup> K]	$R^2$ [-]	AAE [%]	ABE [%]	MAE [W/m <sup>2</sup> K]	MBE [W/m <sup>2</sup> K]
24	3.328	0.0409	298	298	2.18	2.18
25	2.999	0.0426	258	258	1.86	1.86
26	1.305	0.0426	70	56	0.42	0.16
27	1.938	0.0409	132	132	0.80	0.79
28	2.153	0.0409	158	157	1.01	1.00
29	1.933	0.0437	131	131	0.81	0.79
30	1.692	0.0437	105	102	0.61	0.55
31	1.324	0.0415	72	58	0.42	0.18
33	1.271	0.0426	68	52	0.41	0.12
34	1.912	0.0437	129	128	0.79	0.77
35	1.829	0.0436	119	118	0.71	0.69
36	2.563	0.0421	206	206	1.42	1.42
37	2.738	0.0421	227	227	1.60	1.60
38	1.355	0.0426	74	62	0.43	0.21

The results presented here show significant differences between measurements and models. The best degree of convergence between predicted and measured results, given by AAE, was obtained in models given by Equations (26), (31), (33) and (38). MAE ranged from 0.41 W/m<sup>2</sup>K (Equation (33)) to 2.18 W/m<sup>2</sup>K (Equation (24)), showing relatively high deviations from the modelled CHTC versus measurements. The average bias in the models given by MBE varied from 0.12 W/m<sup>2</sup>K (Equation (33)) to 2.18 W/m<sup>2</sup>K (Equation (24)). From these results, it can be stated that the best match with measurements was obtained by the model of Fohanno and Polidori given by Equation (33).

Such discrepancies were also reported in other studies. For example, Kalema and Haapala [7] analysed the impact of interior heat transfer coefficient models on the thermal dynamics of a two-room test cell with radiator heating. Experimental results from the tests under steady-state and dynamic conditions were compared with that simulated in the thermal analysis program TASE. ASHRAE, Alamdari and Hammond, and Khalifa and Marshall correlation equations were used in the calculations of convective heat transfer coefficients. Measured air and surface temperatures were within the simulated minimum-maximum range of 4 °C. Only the window surface temperature was 0.7 °C greater than the calculated maximum temperature. All calculated heat fluxes were within the 10% error band of the measured values.

The discrepancies presented here may have an impact on simulation results when using computer tools for the dynamic simulation of buildings [10]. Commonly in such cases, constant values of internal CHTC and RHTC are assumed. If vertical walls are of interest, in the first case the values within the range from 2.0 W/m<sup>2</sup>K to 5.0 W/m<sup>2</sup>K [87–89] are met.

In the energy auditing of buildings, when monthly calculation methods are applied, constant values of total combined convective and radiative heat transfer coefficient (or internal surface resistance) are normally used [90–92].

In contrast to measured RHTC, it is not easy to present any recommendations on CHTC values to be used based on this study. Further detailed analyses are needed to find and minimise measurement uncertainties. The presented analysis shows that the most important contribution to CHTC uncertainty is the measurement of the temperature difference between internal air and wall surface.

#### 4. Conclusions

In the present study, convective (CHTC) and radiative (RHTC) heat transfer coefficients for the internal surface of a vertical wall were calculated from measurements. For

comparative purposes, in the first case, 14 correlations were used to obtain CHTC from temperature difference and, in several cases, the height of a wall.

The results showed significant differences between measurements and mathematical models. This was likely because in the present study measurements were taken during the everyday use of a building. Hence, it was not possible to obtain the stable thermal conditions possible in the test chambers used in other experimental studies. Moreover, the internal surfaces of the test chambers were covered with materials different from those used in the building. For example, in the study of Khalifa and Marshall [10] authors used aluminium foil on the internal and external surfaces of the external partitions of their climatic chamber. This was employed to minimise the effect of longwave radiation exchange on the temperature and heat flux measurements, and meant that only convective heat transfer was studied. In the present study, combined convective and radiative heat transfer was considered.

It should also be noted that aluminium foil has different physical properties (especially roughness influencing the flow of air) than the cement-lime plaster used as the surface layers of ceramic walls. The flow of air could be also influenced because of stairs located near the sensors. The stairs are about 2 cm away from the wall and their construction allows air to flow, but its presence cannot be excluded from the measurement results.

Model quality was estimated using four statistical goodness-of-fit criteria: AAE, ABE, MAE and MBE. On this basis, the model of Fohanno and Polidori was chosen as the best, with AAE = 68%, ABE = 52%, MAE = 0.41 W/m<sup>2</sup>K and MBE = 0.12 W/m<sup>2</sup>K. The resulting  $h_c = 1.217$  W/m<sup>2</sup>K. The worst model was that of Wilkes and Peterson, for which AAE = 298%, ABE = 298%, MAE = 2.18 W/m<sup>2</sup>K, MBE = 2.18 W/m<sup>2</sup>K and  $h_c = 3.328$  W/m<sup>2</sup>K.

The experiment could be repeated over an extended period to avoid possible temporary disruptions and with the addition of airflow velocity measurement near the wall. Moreover, a shorter sampling time could be used and then time averaging in longer periods could be applied for comparison with hourly values calculated from other models.

The study showed, however, that calculated total surface resistance is close to that recommended by EN ISO 6946 standard, commonly used in energy auditing and certification of buildings. However, it is a rather crude estimation applied in less accurate, annual or monthly methods.

Because of the noticeable impact of a temperature difference between internal air and wall surface on CHTC uncertainty, in future studies, emphasis should be given to this issue.

**Funding:** This research received no external funding.

**Conflicts of Interest:** The authors declare no conflict of interest.

## Symbols

$h_c$	convective heat transfer coefficient, W/m <sup>2</sup> K
$h_m$	measured value of heat transfer coefficient, W/m <sup>2</sup> K
$h_p$	predicted (by the certain correlation) value of heat transfer coefficient, W/m <sup>2</sup> K
$h_r$	radiative heat transfer coefficient, W/m <sup>2</sup> K
$k$	coverage factor, —
$m$	the total number of measurement samples, —
$q_c$	convective heat flux density, W/m <sup>2</sup>
$q_r$	radiative heat flux density, W/m <sup>2</sup>
$q_w$	wall conductive heat flux density, W/m <sup>2</sup>
$u_c$	combined uncertainty, —
$R^2$	coefficient of determination, —
$T_i$	internal air temperature, °C
$T_r$	mean radiant temperature, °C
$T_s$	wall surface temperature, °C

U	expanded uncertainty, —
$\varepsilon$	surface emissivity, —
$\sigma$	Stefan–Boltzmann constant, $\sigma = 5.6697 \cdot 10^{-8} \text{ W/m}^2\text{K}^4$
AAE	average absolute error, %
ABE	average biased error, %
MAE	mean absolute error, $\text{W/m}^2\text{K}$
MBE	mean bias error, $\text{W/m}^2\text{K}$

## References

- Zaim, A.; Aissa, A.; Mebarek-Oudina, F.; Mahanthesh, B.; Lorenzini, G.; Sahnoun, M.; El Ganaoui, M. Galerkin finite element analysis of magneto-hydrodynamic natural convection of Cu-water nanoliquid in a baffled U-shaped enclosure. *Propuls. Power Res.* **2020**, *9*, 383–393. [[CrossRef](#)]
- Abo-Dahab, S.M.; Abdelhafez, M.A.; Mebarek-Oudina, F.; Bilal, S.M. MHD Cassonnanofluid flow over nonlinearly heated porous medium in presence of extending surface effect with suction/injection. *Indian J. Phys.* **2021**, 1–15. [[CrossRef](#)]
- Shafiq, A.; Mebarek-Oudina, F.; Sindhu, T.N.; Abidi, A. A study of dual stratification on stagnation point Walters’B nanofluid flow via radiative Riga plate: A statistical approach. *Eur. Phys. J. Plus* **2021**, *136*, 407. [[CrossRef](#)]
- Palacio-Caro, I.D.; Alvarado-Torres, P.N.; Cardona-Sepúlveda, L.F. Numerical Simulation of the Flow and Heat Transfer in an Electric Steel Tempering Furnace. *Energies* **2020**, *13*, 3655. [[CrossRef](#)]
- Markiewicz-Zahorski, P.; Rucińska, J.; Fedorczak-Cisak, M.; Zielina, M. Building Energy Performance Analysis after Changing Its Form of Use from an Office to a Residential Building. *Energies* **2021**, *14*, 564. [[CrossRef](#)]
- Kwiatkowski, J.; Rucińska, J. Estimation of Energy Efficiency Class Limits for Multi-Family Residential Buildings in Poland. *Energies* **2020**, *13*, 6234. [[CrossRef](#)]
- Kalema, T.; Haapala, T. Effect of interior heat transfer coefficients on thermal dynamics and energy consumption. *Energy Build.* **1995**, *22*, 101–113. [[CrossRef](#)]
- Lomas, K.J. The U.K. applicability study: An evaluation of thermal simulation programs for passive solar house design. *Build. Environ.* **1996**, *31*, 197–206. [[CrossRef](#)]
- Domínguez-Muñoz, F.; Cejudo-López, J.M.; Carrillo-Andrés, A. Uncertainty in peak cooling load calculations. *Energy Build.* **2010**, *42*, 1010–1018. [[CrossRef](#)]
- Obyn, S.; van Moeseke, G. Variability and impact of internal surfaces convective heat transfer coefficients in the thermal evaluation of office buildings. *Appl. Therm. Eng.* **2015**, *87*, 258–272. [[CrossRef](#)]
- Michalak, P.; Szczołka, K.; Szymiczek, J. Energy Effectiveness or Economic Profitability? A Case Study of Thermal Modernization of a School Building. *Energies* **2021**, *14*, 1973. [[CrossRef](#)]
- Walikewitz, N.; Janicke, B.; Langner, M.; Meier, F.; Endlicher, W. The difference between the mean radiant temperature and the air temperature within indoor environments: A case study during summer conditions. *Build. Environ.* **2015**, *84*, 151–161. [[CrossRef](#)]
- Filippin, C.; Beascochea, A. Performance assessment of low-energy buildings in central Argentina. *Energy Build.* **2007**, *39*, 546–557. [[CrossRef](#)]
- Bueno, B.; Norford, L.; Pigeon, G.; Britter, R. A resistance-capacitance network model for the analysis of the interactions between the energy performance of buildings and the urban climate. *Build. Environ.* **2012**, *54*, 116–125. [[CrossRef](#)]
- Herwig, H. What Exactly is the Nusselt Number in Convective Heat Transfer Problems and are There Alternatives? *Entropy* **2016**, *18*, 198. [[CrossRef](#)]
- Bienvenido-Huertas, D.; Bermúdez, J.; Moyano, J.J.; Marín, D. Influence of ICHTC correlations on the thermal characterization of façades using the quantitative internal infrared thermography method. *Build. Environ.* **2019**, *149*, 515–525. [[CrossRef](#)]
- Saunders, O.A. The effect of pressure upon natural convection in air. *Proc. R. Soc. Lond.* **1936**, *157*, 278–291. [[CrossRef](#)]
- Saunders, O.A. Natural convection in liquids. *Proc. R. Soc. Lond.* **1939**, *172*, A17255–A17271. [[CrossRef](#)]
- Fishenden, M.; Saunders, O.A. *An Introduction to Heat Transfer*; Clarendon Press: Oxford, UK, 1950.
- McAdams, W.H. *Heat Transmission*; McGraw-Hill: New York, NY, USA, 1954.
- Lewandowski, W.M.; Kubski, P. Effect of the use of the balance and gradient methods as a result of experimental investigations of natural convection action with regard to the conception and construction of measuring apparatus. *Wärme- Und Stoffübertragung* **1984**, *18*, 247–256. [[CrossRef](#)]
- Lewandowski, W.M. Natural convection heat transfer from plates of finite dimensions. *Int. J. Heat Mass Transf.* **1991**, *34*, 875–885. [[CrossRef](#)]
- Fujii, T.; Imura, H. Natural-convection heat transfer from a plate with arbitrary inclination. *Int. J. Heat Mass Transf.* **1972**, *15*, 755–767. [[CrossRef](#)]
- Churchill, S.W.; Usagi, R. A general expression for the correlation of rates of transfer and other phenomena. *AiChE J.* **1972**, *18*, 1121–1128. [[CrossRef](#)]
- Khalifa, A.J.N.; Marshall, R.H. Validation of heat transfer coefficients on interior building surfaces using a real-sized indoor test cell. *Int. J. Heat Mass Transf.* **1990**, *33*, 2219–2236. [[CrossRef](#)]
- Alamdari, F.; Hammond, G.P. Improved data correlations for buoyancy-driven convection in rooms. *Build. Serv. Eng. Res. Technol.* **1983**, *4*, 106–112. [[CrossRef](#)]

27. Awbi, H.B.; Hatton, A. Natural convection from heated room surfaces. *Energy Build.* **1999**, *30*, 233–244. [[CrossRef](#)]
28. Delaforce, S.R.; Hitchin, E.R.; Watson, D.M.T. Convective heat transfer at internal surfaces. *Build. Environ.* **1993**, *28*, 211–220. [[CrossRef](#)]
29. Sukamto, D.; Siroux, M.; Gloriant, F. Hot Box Investigations of a Ventilated Bioclimatic Wall for NZEB Building Façade. *Energies* **2021**, *14*, 1327. [[CrossRef](#)]
30. Shinoda, J.; Kazanci, O.B.; Tanabe, S.; Olesen, B.W. A review of the surface heat transfer coefficients of radiant heating and cooling systems. *Build. Environ.* **2019**, *159*, 106156. [[CrossRef](#)]
31. Cholewa, T.; Rosiński, M.; Spik, Z.; Dudzińska, M.R.; Siuta-Olcha, A. On the heat transfer coefficients between heated/cooled radiant floor and room. *Energy Build.* **2013**, *66*, 599–606. [[CrossRef](#)]
32. Cholewa, T.; Anasiewicz, R.; Siuta-Olcha, A.; Skwarczynski, M.A. On the heat transfer coefficients between heated/cooled radiant ceiling and room. *Appl. Therm. Eng.* **2017**, *117*, 76–84. [[CrossRef](#)]
33. Acikgoz, O.; Kincay, O. Experimental and numerical investigation of the correlation between radiative and convective heat-transfer coefficients at the cooled wall of a real-sized room. *Energy Build.* **2015**, *108*, 257–266. [[CrossRef](#)]
34. Koca, A.; Gemici, Z.; Topacoglu, Y.; Cetin, G.; Acet, R.C.; Kanbur, B.B. Experimental investigation of heat transfer coefficients between hydronic radiant heated wall and room. *Energy Build.* **2014**, *82*, 211–221. [[CrossRef](#)]
35. Guo, R.; Heiselberg, P.; Hu, Y.; Johra, H.; Zhang, C.; Jensen, R.L.; Jönsson, K.T.; Peng, P. Experimental investigation of convective heat transfer for night cooling with diffuse ceiling ventilation. *Build. Environ.* **2021**, *193*, 107665. [[CrossRef](#)]
36. Guo, R.; Heiselberg, P.; Hu, Y.; Johra, H.; Zhang, C.; Jensen, R.L.; Jönsson, K.T.; Peng, P. Experimental investigation of convective heat transfer for night ventilation in case of mixing ventilation. *Build. Environ.* **2021**, *193*, 107670. [[CrossRef](#)]
37. Peeters, L.; Beausoleil-Morrison, I.; Novoselac, A. Internal convective heat transfer modeling: Critical review and discussion of experimentally derived correlations. *Energy Build.* **2011**, *43*, 2227–2239. [[CrossRef](#)]
38. Camci, M.; Karakoyun, Y.; Acikgoz, O.; Dalkilic, A.S. A comparative study on convective heat transfer in indoor applications. *Energy Build.* **2021**, *242*, 110985. [[CrossRef](#)]
39. Khalifa, A.J.N. Natural convective heat transfer coefficient—A review: I. Isolated vertical and horizontal surfaces. *Energy Convers. Manag.* **2001**, *42*, 491–504. [[CrossRef](#)]
40. Khalifa, A.J.N. Natural convective heat transfer coefficient—A review: II. Surfaces in two- and three-dimensional enclosures. *Energy Convers. Manag.* **2001**, *42*, 505–517. [[CrossRef](#)]
41. Dagtekin, I.; Oztop, H.F. Natural convection heat transfer by heated partitions within enclosure. *Int. Commun. Heat Mass Transf.* **2001**, *28*, 823–834. [[CrossRef](#)]
42. Vollaro, A.D.L.; Galli, G.; Vallati, A. CFD Analysis of Convective Heat Transfer Coefficient on External Surfaces of Buildings. *Sustainability* **2015**, *7*, 9088–9099. [[CrossRef](#)]
43. Zhong, W.; Zhang, T.; Tamura, T. CFD Simulation of Convective Heat Transfer on Vernacular Sustainable Architecture: Validation and Application of Methodology. *Sustainability* **2019**, *11*, 4231. [[CrossRef](#)]
44. Berrabah, S.; Moussa, M.O.; Bakhouya, M. 3D Modeling of the Thermal Transfer through Precast Buildings Envelopes. *Energies* **2021**, *14*, 3751. [[CrossRef](#)]
45. Maragkos, G.; Beji, T. Review of Convective Heat Transfer Modelling in CFD Simulations of Fire-Driven Flows. *Appl. Sci.* **2021**, *11*, 5240. [[CrossRef](#)]
46. Kaminska, A. Impact of Heating Control Strategy and Occupant Behavior on the Energy Consumption in a Building with Natural Ventilation in Poland. *Energies* **2019**, *12*, 4304. [[CrossRef](#)]
47. Lundström, L.; Akander, J.; Zambrano, J. Development of a Space Heating Model Suitable for the Automated Model Generation of Existing Multifamily Buildings—A Case Study in Nordic Climate. *Energies* **2019**, *12*, 485. [[CrossRef](#)]
48. EN 1264. *Water Based Surface Embedded Heating and Cooling Systems*; SIST: Bratislava, Slovakia, 2011.
49. ISO 11855. *Building Environment Design—Design, Dimensioning, Installation and Control of Embedded Radiant Heating and Cooling Systems*; ISO: Geneva, Switzerland, 2012.
50. EN ISO 6946. *Building Components and Building Elements—Thermal Resistance and Thermal Transmittance—Calculation Methods*; ISO: Geneva, Switzerland, 2007.
51. ASHRAE. *Handbook HVAC Fundamentals*; ASHRAE: New York, NY, USA, 2009.
52. François, A.; Ibos, L.; Feuillet, V.; Meulemans, J. Novel in situ measurement methods of the total heat transfer coefficient on building walls. *Energy Build.* **2020**, *219*, 110004. [[CrossRef](#)]
53. Wallentén, P. Convective heat transfer coefficients in a full-scale room with and without furniture. *Build. Environ.* **2001**, *36*, 743–751. [[CrossRef](#)]
54. Helm, I.; Jalukse, L.; Leito, I. Measurement Uncertainty Estimation in Amperometric Sensors: A Tutorial Review. *Sensors* **2010**, *10*, 4430–4455. [[CrossRef](#)]
55. Ohlsson, K.E.A.; Östin, R.; Olofsson, T. Accurate and robust measurement of the external convective heat transfer coefficient based on error analysis. *Energy Build.* **2016**, *117*, 83–90. [[CrossRef](#)]
56. Chen, J.; Chen, C. Uncertainty Analysis in Humidity Measurements by the Psychrometer Method. *Sensors* **2017**, *17*, 368. [[CrossRef](#)]
57. Chen, L.-H.; Chen, J.; Chen, C. Effect of Environmental Measurement Uncertainty on Prediction of Evapotranspiration. *Atmosphere* **2018**, *9*, 400. [[CrossRef](#)]

58. Jing, H.; Quan, Z.; Zhao, Y.; Wang, L.; Ren, R.; Liu, Z. Thermal Performance and Energy Saving Analysis of Indoor Air–Water Heat Exchanger Based on Micro Heat Pipe Array for Data Center. *Energies* **2020**, *13*, 393. [CrossRef]
59. Ali, A.; Cocchi, L.; Picchi, A.; Facchini, B. Experimental Determination of the Heat Transfer Coefficient of Real Cooled Geometry Using Linear Regression Method. *Energies* **2021**, *14*, 180. [CrossRef]
60. Ficker, T. Virtual emissivities of infrared thermometers. *Infrared Phys. Technol.* **2021**, *114*, 103656. [CrossRef]
61. Chen, H.-Y.; Chen, C. Determining the emissivity and temperature of building materials by infrared thermometer. *Constr. Build. Mater.* **2016**, *126*, 130–137. [CrossRef]
62. Höser, D.; Wallimann, R.; von Rohr, P.R. Uncertainty Analysis for Emissivity Measurement at Elevated Temperatures with an Infrared Camera. *Int. J. Thermophys.* **2016**, *37*, 14. [CrossRef]
63. Zribi, A.; Barthès, M.; Bégot, S.; Lanzetta, F.; Rauch, J.Y.; Moutarlier, V. Design, fabrication and characterization of thin film resistances for heat flux sensing application. *Sens. Actuators A Phys.* **2016**, *245*, 26–39. [CrossRef]
64. Heat Flux Plate/Heat Flux Sensor HFP01 & HFP03. User Manual. Hukseflux Manual v1721. Available online: [https://www.hukseflux.com/uploads/product-documents/HFP01\\_HFP03\\_manual\\_v1721.pdf](https://www.hukseflux.com/uploads/product-documents/HFP01_HFP03_manual_v1721.pdf) (accessed on 25 August 2021).
65. Evangelisti, L.; Guattari, C.; Gori, P.; de LietoVollaro, R.; Asdrubali, F. Experimental investigation of the influence of convective and radiative heat transfers on thermal transmittance measurements. *Int. Commun. Heat Mass Transf.* **2016**, *78*, 214–223. [CrossRef]
66. Bienvenido-Huertas, D.; Moyano, J.; Rodríguez-Jiménez, C.E.; Muñoz-Rubio, A.; Bermúdez Rodríguez, F.J. Quality Control of the Thermal Properties of Superstructures in Accommodation Spaces in Naval Constructions. *Sustainability* **2020**, *12*, 4194. [CrossRef]
67. Fohanno, S.; Polidori, G. Modelling of natural convective heat transfer at an internal surface. *Energy Build.* **2006**, *38*, 548–553. [CrossRef]
68. Musy, M.; Wurtz, E.; Winkelmann, F.; Allard, F. Generation of a zonal model to simulate natural convection in a room with a radiative/convective heater. *Build. Environ.* **2001**, *36*, 589–596. [CrossRef]
69. Rogers, G.F.C.; Mayhew, Y.R. *Engineering Thermodynamics. Work and Heat Transfer*; Pearson Education Ltd.: London, UK, 1992.
70. Michalak, P. The development and validation of the linear time varying Simulink-based model for the dynamic simulation of the thermal performance of buildings. *Energy Build.* **2017**, *141*, 333–340. [CrossRef]
71. Yin, C.-Y. Prediction of higher heating values of biomass from proximate and ultimate analyses. *Fuel* **2011**, *90*, 1128–1132. [CrossRef]
72. Qian, X.; Lee, S.; Soto, A.-M.; Chen, G. Regression Model to Predict the Higher Heating Value of Poultry Waste from Proximate Analysis. *Resources* **2018**, *7*, 39. [CrossRef]
73. Lauster, M.; Teichmann, J.; Fuchs, M.; Streblow, R.; Mueller, D. Low order thermal network models for dynamic simulations of buildings on city district scale. *Build. Environ.* **2014**, *73*, 223–231. [CrossRef]
74. Cui, Y.; Xie, J.; Liu, J.; Xue, P. Experimental and Theoretical Study on the Heat Transfer Coefficients of Building External Surfaces in the Tropical Island Region. *Appl. Sci.* **2019**, *9*, 1063. [CrossRef]
75. Gaši, M.; Milovanović, B.; Gumbarević, S. Comparison of Infrared Thermography and Heat Flux Method for Dynamic Thermal Transmittance Determination. *Buildings* **2019**, *9*, 132. [CrossRef]
76. Samardzioska, T.; Apostolska, R. Measurement of Heat-Flux of New Type Façade Walls. *Sustainability* **2016**, *8*, 1031. [CrossRef]
77. De Rubeis, T.; Muttillio, M.; Nardi, I.; Pantoli, L.; Stornelli, V.; Ambrosini, D. Integrated Measuring and Control System for Thermal Analysis of Buildings Components in Hot Box Experiments. *Energies* **2019**, *12*, 2053. [CrossRef]
78. Lihakanga, R.; Ding, Y.; Medero, G.M.; Chapman, S.; Goussetis, G. A High-Resolution Open Source Platform for Building Envelope Thermal Performance Assessment Using a Wireless Sensor Network. *Sensors* **2020**, *20*, 1755. [CrossRef]
79. Tejedor, B.; Gaspar, K.; Casals, M.; Gangoles, M. Analysis of the Applicability of Non-Destructive Techniques to Determine In Situ Thermal Transmittance in Passive House Façades. *Appl. Sci.* **2020**, *10*, 8337. [CrossRef]
80. Ambrožová, K.; Hrbáček, F.; Láška, K. The Summer Surface Energy Budget of the Ice-Free Area of Northern James Ross Island and Its Impact on the Ground Thermal Regime. *Atmosphere* **2020**, *11*, 877. [CrossRef]
81. Mosayebidorcheh, S.; Ganji, D.D.; Farzinpoor, M. Approximate solution of the nonlinear heat transfer equation of a fin with the power-law temperature-dependent thermal conductivity and heat transfer coefficient. *Propuls. Power Res.* **2014**, *3*, 41–47. [CrossRef]
82. Qian, X.; Xue, J.; Yang, Y.; Lee, S.W. Thermal Properties and Combustion-Related Problems Prediction of Agricultural Crop Residues. *Energies* **2021**, *14*, 4619. [CrossRef]
83. Ficco, G.; Frattolillo, A.; Malengo, A.; Puglisi, G.; Saba, F.; Zuena, F. Field verification of thermal energy meters through ultrasonic clamp-on master meters. *Measurement* **2020**, *151*, 107152. [CrossRef]
84. Ficco, G.; Iannetta, F.; Ianniello, E.; d’AmbrosioAlfano, F.R.; Dell’Isola, M. U-value in situ measurement for energy diagnosis of existing buildings. *Energy Build.* **2015**, *104*, 108–121. [CrossRef]
85. Gil, B.; Rogala, Z.; Dorosz, P. Pool Boiling Heat Transfer Coefficient of Low-Pressure Glow Plasma Treated Water at Atmospheric and Reduced Pressure. *Energies* **2020**, *13*, 69. [CrossRef]
86. Michalak, P. Annual Energy Performance of an Air Handling Unit with a Cross-Flow Heat Exchanger. *Energies* **2021**, *14*, 1519. [CrossRef]
87. Kämpf, J.H.; Robinson, D. A simplified thermal model to support analysis of urban resource flows. *Energy Build.* **2007**, *39*, 445–453. [CrossRef]

88. Ben-Nakhi, A.E.; Aasem, E.O. Development and integration of a user friendly validation module within whole building dynamic simulation. *Energy Convers. Manag.* **2003**, *44*, 53–64. [[CrossRef](#)]
89. Mahdaoui, M.; Hamdaoui, S.; Ait Msaad, A.; Kousksou, T.; El Rhafiki, T.; Jamil, A.; Ahachad, M. Building bricks with phase change material (PCM): Thermal performances. *Constr. Build. Mater.* **2021**, *269*, 121315. [[CrossRef](#)]
90. Dobrzycki, A.; Kurz, D.; Mikulski, S.; Wodnicki, G. Analysis of the Impact of Building Integrated Photovoltaics (BIPV) on Reducing the Demand for Electricity and Heat in Buildings Located in Poland. *Energies* **2020**, *13*, 2549. [[CrossRef](#)]
91. Babiarsz, B.; Szymański, W. Introduction to the Dynamics of Heat Transfer in Buildings. *Energies* **2020**, *13*, 6469. [[CrossRef](#)]
92. Jezierski, W.; Sadowska, B.; Pawłowski, K. Impact of Changes in the Required Thermal Insulation of Building Envelope on Energy Demand, Heating Costs, Emissions, and Temperature in Buildings. *Energies* **2021**, *14*, 56. [[CrossRef](#)]